Analysis of Energy Transfer Efficiency in UAV-Enabled Wireless Networks

Hua Yan, Yunfei Chen, Shuang-Hua Yang

Abstract

Wireless power transfer (WPT) is a promising charging technology for battery-limited sensors. In this paper, we study the energy transfer in a wireless network using an unmanned aerial vehicle (UAV). Instead of charging the remote wireless sensors directly from the access point (AP), we study the schemes of using a UAV to charge the remote wireless sensors after it is charged by the AP. To this end, two schemes are proposed. The performances of these two schemes are examined and compared with the conventional scheme without using a UAV. A distance threshold beyond which the new schemes have superiority over the conventional scheme is derived by solving energy equations. Numerical results show that the proposed schemes can achieve significantly higher energy efficiency than the conventional scheme when the transmission distance is within the derived critical range.

Index Terms

Energy efficiency, energy harvesting, radio frequency, unmanned aerial vehicle, wireless power transfer.

I. Introduction

In recent years, there has been increasing popularity in unmanned aerial vehicles (UAVs), as it has been widely used in many public, military and civil applications [1] – [3]. For example, UAVs have been

H. Yan is with the School of Engineering, University of Warwick, Coventry, CV4 7AL, U.K. (e-mail: Hua.Yan@warwick.ac.uk)

Y. Chen is with the School of Engineering, University of Warwick, Coventry, CV4 7AL, U.K. (e-mail: Yunfei.Chen@warwick.ac.uk)

S. Yang is with the Department of Computer Science and Engineering, Southern University of Science and Technology, Shenzhen 518000, China, and also with the Department of Computer Science, Loughborough University, Loughborough LE11 3TU, U.K. (e-mail: yangsh@sustc.edu.cn or s.h.yang@lboro.ac.uk)

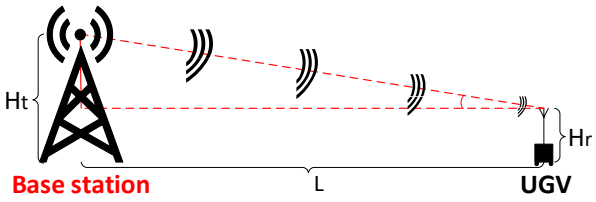

Fig. 1. The conventional direct energy transfer scheme.

adopted in environmental and natural disaster monitoring, for area or network coverage, as aerial base stations (BSs) or relays, and for delivery of goods and construction.

In particular, as an aerial BS or relay, UAVs play a very important role in UAV-enabled wireless networks. The authors in [4] optimized the altitude of a low-altitude aerial platform (LAP) to provide the maximum radio coverage for the ground users. In [5], the authors considered this problem in a relaying setting and studied the optimum placement of a relaying UAV for the maximum reliability. Furthermore, works on mobile relaying and mobile BS were also studied in [6] and [7], respectively. Zeng *et al.* [6] studied the throughput maximization problem in mobile relaying system by optimizing the transmit power, while Lyu *et al.* [7] focused on minimizing the number of mobile BSs needed to provide effective wireless coverage for several distributed ground terminals so that each ground terminal can have an effective communication connection with the mobile BS. In the seminal paper [8], the authors proposed a new cyclical multiple access (CMA) scheme to explore the periodic channel variations between a mobile BS served by a UAV and ground terminals for maximum throughput. The results show that there exists a trade-off between throughput and access delay in their proposed CMA scheme. For UAV relaying networks or systems, the authors in [9] jointly investigated the optimization problem of UAV node placement and communication resource allocation to achieve the maximum throughput. In [10], a solution that jointly optimizes trajectory design and power control was proposed to minimize the outage probability of the UAV relaying network. All of the above works have provided very useful insights on the applications of UAV as a relay or a BS to provide information relay or information coverage. However, energy is as important as information in communications systems, especially in wireless sensor networks where the sensors are of limited battery life.

There have also been a large amount of literature on UAV-enabled wireless power transfer (WPT). For example, in [11], a WPT system with a UAV-mounted energy transmitter was considered and for a basic two-user scenario, the energy region and the amount of energy transferred over a fixed period of time was studied jointly with the mobility and trajectory design of the UAV. In [12], the authors extended the two-

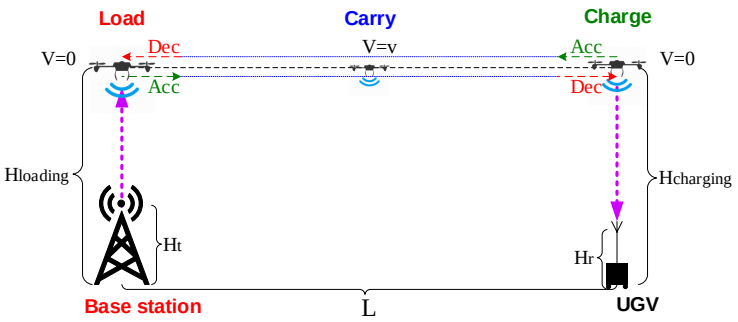

Fig. 2. The proposed Scheme 1.

user scenario to more users and improved the minimum energy by optimizing the trajectory of the UAV. In [13], both UAV's optimal hovering locations for the sum-energy maximization and UAV's optimal hovering time allocations for maximizing the minimum received energy among all energy receivers were investigated by trajectory optimization. In [14], a one-dimensional UAV trajectory was designed for a multi-user WPT system. Also, reference [15] considered a two-user scenario, but the UAV was equipped with a directional antenna for improving the energy transfer efficiency. In [16], the scenario was further extended to the case of multi-UAVs and multiple ground users, and the throughput was maximized by optimizing the user scheduling through considering the UAV trajectory and power control jointly. In [17], energy harvesting amplify-and-forward (AF) relaying network was considered, where the UAV acts as a relay. Reference [18] studied the energy trade-off between the uplink transmission energy of the ground terminals and the propulsion energy for UAV's movement. Other works include the related technologies, principles and applications of wireless charging in [19] – [24], radio frequency (RF) energy models and energy transfer channel models in [25] – [26], mobile charging technologies [27] – [29], wireless energy harvesting [30] and propulsion power consumption model for rotary-wing UAV [31]. In [32], the authors considered a framework for UAV-assisted wireless charging of sensor nodes using RF energy transfer. All these works have considered the scenario where the UAV acts as a traditional static relay or an aerial BS to provide energy relay or energy coverage by WPT. However, a realistic and important issue that has been largely ignored is the power consumption of UAV. Some of these works (i.e., [13], [14], [15] and [17]) have also ignored the RF-to-direct current (DC) energy conversion efficiency at energy receivers. Besides, the path loss caused by the transmission distance seriously reduces the energy transfer efficiency. To improve the energy transfer efficiency, one efficient method is to reduce the path loss caused by long transmission distance. For this purpose, one interesting work is data ferry, where a third transceiver receives the data from the BS in its close proximity and then carry the data to the sensors for another

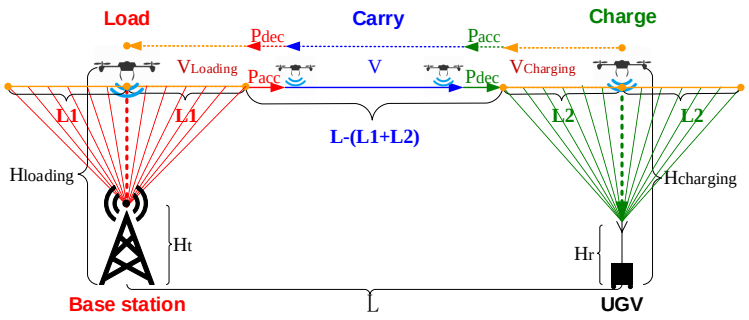

Fig. 3. The proposed Scheme 2.

transmission in close proximity. For example, in [33], the authors considered the method of using one or more UAVs to relay messages between two distant ground nodes. A "load-carry-and-deliver" (LCAD) paradigm was proposed to let the UAV load data from a source node, carry the data to the destination node, and finally deliver the data to the destination node. It has been shown in these works that data ferry is more efficient than traditional direct transmission. Moreover, works on cooperative communications, such as two-way multi-antenna cooperative relaying with comparison of one-hop direct transmission and two-hop relay-aided transmission [34] – [38], have also provided very valuable insights on relay-aided transmission strategies, and it is interesting to use UAV as a mobile relay following the idea of these works.

Motivated by the above observations, in this paper, we study the WPT efficiency in a UAV-enabled wireless network, where a UAV is used to charge the remote unmanned ground vehicle (UGV). We propose two new schemes for UAV-enabled WPT. The new and conventional schemes (long distance direct wireless charging without using a UAV) are compared by analysing their RF energy transfer model, UAV energy consumption model and RF-to-DC conversion efficiency model. A critical distance beyond which the new schemes have a higher energy transfer efficiency than the conventional direct charging is derived. Numerical results are presented to show the influences of the RF-to-DC conversion efficiency and the UAV flight height on the critical distance of the new schemes. Specifically, the critical distance is reduced from $192.99\ m$ to $75.0\ m$ when the RF-to-DC conversion efficiency increases from 0.6 to 1.0 for a fixed UAV height of $6.4\ m$ above ground level. Also, when the RF-to-DC conversion efficiency is set to 0.6, the critical distance increases from about $59.69\ m$ to $192.99\ m$ when the UAV height increases from $6.0\ m$ to $6.4\ m$. The main contributions of this work can be summarized as follows:

- We propose two new schemes for UAV-enabled WPT in wireless networks.
- We derive and quantify the exact critical distance and the effective range beyond which the new

schemes have superiority over the conventional direct charging.

- We examine the effects of different system parameters on the performance of the proposed schemes to give useful guidance for system designs.

The rest of the paper is organized as follows. In Section II, the system models used in the proposed schemes are introduced. The new schemes and the critical distance are studied in Section III. Numerical results are presented in Section IV. Finally, we conclude the work in Section V. Some frequently used symbols in this paper are summarized in Table I.

Table I: Symbols in the paper

Notations	**Description**
L_{FS}^{s1-1}	path loss from the BS to the UAV in Scheme 1
L_{FS}^{s1-2}	path loss from the UAV to the UGV in Scheme 1
L_{FS}^{s2-1}	path loss from the BS to the UAV in Scheme 2
L_{FS}^{s2-2}	path loss from the UAV to the UGV in Scheme 2
d_{s1-1}	transmission distance from the BS to the UAV in Scheme 1
d_{s1-2}	transmission distance from the UAV to the UGV in Scheme 1
d_{s2-1}	transmission distance from the BS to the UAV in Scheme 2
d_{s2-2}	transmission distance from the UAV to the UGV in Scheme 2
L_1	horizontal distance on both sides of the BS during the $load$ stage
L_2	horizontal distance on both sides of the UGV during the $charge$ stage
P_{uav-r}^{s1}	received RF power at the UAV in Scheme 1
P_{uav-r}^{s2}	received RF power at the UAV in Scheme 2
P_{uav-t}^{s1}	transmit RF power from the UAV in Scheme 1
P_{uav-t}^{s2}	transmit RF power from the UAV in Scheme 2
P_{ugv}^{s1}	received RF power at the UGV in Scheme 1
P_{ugv}^{s2}	received RF power at the UGV in Scheme 2
E_{uav-DC}^{s1}	received DC energy of UAV from the BS in Scheme 1
E_{uav-DC}^{s2}	received DC energy of UAV from the BS in Scheme 2
E_{fly-to}^{s1}	energy consumption during the $carry$ stage in Scheme 1
E_{fly-to}^{s2}	energy consumption during the $carry$ stage in Scheme 2
$E_{fly-back}^{s1}$	energy consumption for flying back in Scheme 1
$E_{fly-back}^{s2}$	energy consumption for flying back in Scheme 2

II. System Model

Consider three wireless charging scenarios as depicted in Fig. 1, Fig. 2 and Fig.3. In Fig. 1, an unmanned ground vehicle (UGV), located L meters away from the BS, is charged via direct RF energy

transfer. This is the conventional direct energy transfer scheme. In Fig. 2 and Fig. 3, a multi-rotor UAV is used to load the energy near the BS and then deliver the energy to the UGV by charging it from a short distance. These are the two new schemes.

To determine which scheme is more energy efficient, we need to know the energy consumption of different parts of the system. For the conventional scheme, the energy consumption only comes from the transmission loss from the BS to the UGV and the conversion loss from RF to DC at the UGV. For the proposed schemes, the energy consumption comes from the transmission loss from the BS to the UAV and from the UAV to the UGV, the conversion loss from RF to DC at the UAV and at the UGV, and the UAV internal loss due to hovering, acceleration, deceleration and flying operations.

A. Transmission Loss

We assume a line-of-sight (LoS) communication link between the BS and the UAV, and between the UAV and the UGV as in [11]– [15]. Also, the communication link between the BS and the UGV comes with extra power loss caused by shadowing and non-LoS (NLoS). Denote the heights of the BS and the UGV as H_t and H_r, respectively. According to the free-space path loss (FSPL) model [39], the transmission loss L_{FS} is expressed as

$$L_{FS(dB)} = 20\log_{10}\{f_c\} + 20\log_{10}\{d\} - 147.55\ dB, \tag{1}$$

where d $(d \geq 1\ m)$ is the distance between the transmitter and the receiver and f_c is the operating frequency.

In Fig. 1, for the conventional direct transfer scheme, since the distance between the BS and the UGV is L, one has

$$d_0 = \sqrt{L^2 + (H_t - H_r)^2}, d_0 \geq 1\ m. \tag{2}$$

Hence, the transmission loss is

$$L^c_{FS(dB)} = 20\log_{10}\{f_c\} + 20\log_{10}\{d_0\} - 147.55 + X\ dB, \tag{3}$$

where X represents the extra power loss caused by shadowing.

In Fig. 2, for the proposed Scheme 1, the transmission distance from the BS to the UAV is

$$d_{s1-1} = H_{loading} - H_t,\ d_{s1-1} \geq 1\ m, \tag{4}$$

and the distance from the UAV to the UGV is

$$d_{s1-2} = H_{charging} - H_r,\ d_{s1-2} \geq 1\ m. \tag{5}$$

Where $H_{loading} > H_t$ and $H_{charging} > H_r$. Therefore, the transmission loss from the BS to the UAV can be expressed as

$$L_{FS(dB)}^{s1-1} = 20\log_{10}\{f_c\} + 20\log_{10}\{d_{s1-1}\} - 147.55\ dB, \tag{6}$$

and the transmission loss from the UAV to the UGV can be expressed as

$$L_{FS(dB)}^{s1-2} = 20\log_{10}\{f_c\} + 20\log_{10}\{d_{s1-2}\} - 147.55\ dB. \tag{7}$$

For the proposed Scheme 2 in Fig. 3, the UAV is charged while flying over the horizontal distance of L_1 meters on both sides of the BS. We denote each L_1 meters as one flight. Then, the flights within a horizontal distance of L_1 on both sides of the BS are symmetric, and thus we only need to consider the process within one L_1 meter distance. In essence, Scheme 2 charges and discharges the UAV while it is flying instead of hovering. In order to simplify the calculation, we use the average speed of $v_{loading}$ to approximatively calculate the energy obtained during the $load$ stage. Since the UAV flies at a fixed speed of $v_{loading}$ around the BS within a distance of L_1 meters during loading and we denote the instant time within L_1 meters as t, the instantaneous transmission distance at time instant t from the BS to the UAV can be expressed as

$$d_{s2-1}(t) = \sqrt{\left(H_{loading} - H_t\right)^2 + \left(L_1 - v_{loading}t\right)^2}, \tag{8}$$

where $H_{loading} > H_t$ and $L_1 \geq v_{loading}t$ so that $0 \leq t \leq \frac{L_1}{v_{loading}}$, and $d_{s2-1}(t) \geq 1\ m$. Similarly, if the UAV flies at a fixed speed of $v_{charging}$ around the UGV within a distance of L_2 meters during charging, the instantaneous transmission distance at time instant t from the UAV to the UGV can be expressed as

$$d_{s2-2}(t) = \sqrt{\left(H_{charging} - H_r\right)^2 + \left(L_2 - v_{charging}t\right)^2}, \tag{9}$$

where $H_{charging} > H_r$ and $L_2 \geq v_{charging}t$ so that $0 \leq t \leq \frac{L_2}{v_{charging}}$, and $d_{s2-2}(t) \geq 1\ m$. Accordingly, the instantaneous transmission loss from the BS to the UAV can be expressed as

$$L_{FS(dB)}^{s2-1}(t) = 20\lg(f_c) + 20\lg(d_{s2-1}(t)) - 147.55\ dB, \tag{10}$$

and the instantaneous transmission loss from the UAV to the UGV can be expressed as

$$L_{FS(dB)}^{s2-2}(t) = 20\lg(f_c) + 20\lg(d_{s2-2}(t)) - 147.55\ dB. \tag{11}$$

B. UAV Internal Loss

In [40], the authors reported some computational models for the energy consumed by a UAV for its various maneuvers (i.e. hovering, acceleration, deceleration and flying) based on experimental results. We will use these models here. Assume that the energy consumption during UAV acceleration is E_{acc}, and

during UAV deceleration is E_{dec}. Also, E_{hover} and E_v denote energy consumption during hovering and during normal flight at an average speed of v, respectively. According to the results in [40], the internal energy consumption at the UAV during different maneuvers can be calculated as

$$E_{hover} = P_{hover} t_1, \tag{12}$$

$$E_{acc} = P_{\overline{acc}} \left(t_2 - t_1\right), \tag{13}$$

$$E_v = P_v \left(t_3 - t_2\right), \tag{14}$$

$$E_{dec} = P_{\overline{dec}} \left(t_4 - t_3\right), \tag{15}$$

where P_{hover} (watt) is the hovering power, $P_{\overline{acc}}$ (watt) is the average acceleration power, P_v (watt) is the average flying power at a speed of v and $P_{\overline{dec}}$ (watt) is the average deceleration power. Also, t_1 is the hovering time at a speed of 0, $t_2 - t_1$ is the acceleration time, $t_3 - t_2$ is the flying time at a speed of v, and $t_4 - t_3$ is the deceleration time. In this case, the UAV hovers for t_1 seconds, followed by an acceleration for $t_2 - t_1$ seconds to a fixed speed of v, a flying time of $t_3 - t_2$ and finally a deceleration for $t_4 - t_3$ seconds to become static again.

For the proposed Scheme 1 in Fig. 2, the UAV hovers above the BS for charging, then accelerates to a constant speed of v to deliver the energy. When it is close to the UGV, the UAV decelerates and then hovers above the UGV to deliver the energy before flying back to the BS. Thus, hovering, acceleration, deceleration and flying are the only four operations that need to be considered for this scheme.

For the proposed Scheme 2 In Fig. 3, the UAV flies at a fixed speed of $v_{loading}$ around the BS within a distance of L_1 meters for charging, then accelerates to a constant speed of v to carry the energy. When it flies close to the UGV, it decelerates to a fixed speed of $v_{charging}$ and within a distance of L_2 meters for energy delivery before flying back to the BS. Hence, flying (i.e. at a fixed speed of $v_{loading}$, v and $v_{charging}$, respectively), acceleration and deceleration are the only three operations that need to be considered for this scheme. No hovering is performed in this case.

C. RF-to-DC Conversion Loss

In [41] and [42], the authors derived new models for the RF-to-DC conversion efficiency. Because the linear model has been adopted in most existing works and it can simplify the calculation without affecting the simulation results, we will use it here. Assume that the input power is denoted as P_{in}, and that the constant RF-to-DC conversion efficiency is η. Therefore, the RF-to-DC conversion model can be expressed as

$$P_{out} = \eta * P_{in}. \tag{16}$$

III. The Proposed New Schemes

In this section, two wireless charging schemes using RF energy harvesting are proposed, where a UAV used as a carrier is studied. Specifically, four different cases, a conventional scheme with a single UGV, the new schemes with a single UAV, the conventional scheme with multiple UGVs and the new schemes with multiple UGVs, will be compared and discussed.

A. Conventional scheme with a single UGV

In this case, the RF energy from the BS is harvested by a single UGV located L meters away directly, as shown in Fig. 1. Accordingly, the received RF power at the UGV can be expressed as

$$P_{ugv} = \ P_t + G_t + G_{ugv} - 20\text{lg}\left\{f_c\right\} - 20\text{lg}\left\{d_0\right\} + 147.55 - X \ dB, \tag{17}$$

where P_{ugv} (dB) is the received RF power at the UGV, P_t (dB) is the transmit power, G_t and G_{ugv} are the transmitting antenna gain and receiving antenna gain (dBi), respectively, X is the extra power loss, $d_0 = \sqrt{L^2 + (H_t - H_r)^2}$ is the transmission distance between the BS and the UGV, and the transmission loss $L^c_{FS(dB)}$ in (1) has been used here. If the charging time is denoted as $T_{loading}$, the converted DC energy at the UGV is

$$E_{ugv\_DC} = \eta E_{ugv\_RF} = \eta 10^{\frac{P_{ugv}}{10}} T_{loading}, \tag{18}$$

where η is the constant RF-to-DC conversion efficiency defined in (16) and $T_{loading}$ is the loading time which equals to the charging time in this case. Note that, when P_t and $T_{loading}$ are fixed, the received DC energy is affected by the path loss, which is mainly determined by the transmission distance.

B. New Schemes with a Single UGV

For the new schemes. a UAV is used to charge the remote wireless sensors after it is charged by the BS. This method reduces the transmission distance and therefore may be more energy-efficient due to the reduced path loss. In this case, the UAV has to hover above the BS to be charged by the BS. After it has been charged, it flies towards the UGV and then hovers above the UGV to charge the UGV. Fig. 2 and Fig. 3 illustrate the process of the proposed new schemes.

From Fig. 2 and Fig. 3, the process of the new schemes can be divided into three stages: $load$, $carry$ and $charge$, which is similar to the paradigm in [33] for data ferry. In the first stage, the UAV is charged with certain amount of energy by the BS. This is the $load$ stage. The second stage is the $carry$ stage in which the UAV carries the stored energy and flies towards the UGV. Then, the UGV will be powered by the UAV. This is the $charge$ stage. We consider the two different schemes in the following.

1) The Proposed Scheme 1 in Fig. 2:

a) Load: During the first stage, the UAV stays static above the BS at a height of $H_{loading}$. In this case, the received RF power at the UAV can be expressed as

$$P_{uav-r}^{s1} = P_t + G_t + G_{uav} - L_{FS(dB)}^{s1-1}, \tag{19}$$

where G_{uav} is either transmitting or receiving antenna gain of the UAV and P_{uav-r}^{s1} (dB) is the received RF power at the UAV. $L_{FS(dB)}^{s1-1}$ is the transmission loss from the BS to the UAV in (6). Then, the received DC energy is

$$E_{uav-DC}^{s1} = \eta 10^{\frac{P_{uav-r}^{s1}}{10}} T_{loading}^{s1}. \tag{20}$$

Note that, during the $load$ stage, the UAV hovering operation consumes energy as well, because it has to stay above the BS with a power of P_{hover} (dB). This energy consumption can be calculated as

$$E_{hover}^{s1} = P_{hover} T_{loading}^{s1}. \tag{21}$$

Besides, in order to ensure that the UAV does not fall and is in the state of charge, the received DC power should be greater than the hovering power P_{hover}. i.e., $\eta 10^{\frac{P_{uav-r}^{s1}}{10}} > P_{hover}$.

b) Carry: During the second stage, an *acceleration-fly-deceleration* operation of the UAV will be performed to carry energy to the destination. The energy consumption of the $carry$ stage can be calculated as

$$E_{fly-to}^{s1} = \begin{cases} E_{acc}^{s1} + E_{v}^{s1} + E_{dec}^{s1} = P_{\overline{acc}}^{s1}\left(\frac{v}{a}\right) + P_{v}^{s1}\frac{\left(L - \frac{v^2}{a}\right)}{v} + P_{\overline{dec}}^{s1}\left(\frac{v}{a}\right), L > \frac{v^2}{a}, \\ E_{acc}^{s1} + E_{v}^{s1} + E_{dec}^{s1} = P_{\overline{acc}}^{s1}\left(\frac{v}{a}\right) + P_{\overline{dec}}^{s1}\left(\frac{v}{a}\right), L \leq \frac{v^2}{a} \end{cases} \tag{22}$$

where v is the final constant flight speed, a is the acceleration and L is the total distance from the BS to the UGV. Note that, there is no *carry* stage when $L \leq \frac{v^2}{a}$ from (22). Since the UAV needs to fly back to its initial position after each delivery, to ensure that the UAV has enough energy to fly back, the energy consumption for flying back should at least be the same as that for flying to the destination. Thus, this energy consumption of flying back can be given by $E_{fly-back}^{s1} = E_{fly-to}^{s1}$, assuming that the flying back operation is symmetric to the flying to operation.

c) Charge: In the third stage, the UAV is hovering above the UGV at a height of H_{charge} , which is chosen to be the same as the height of loading $H_{loading}$ in the first stage to reduce flight distance and simplify the flight process because we are not aiming at trajectory optimization [10] – [16]. Then, the UAV charges the UGV with a transmitted RF power of P_{uav-t}^{s1} (dB). In this way, the received RF power at the UGV can be derived as

$$P_{ugv}^{s1} = P_{uav-t}^{s1} + G_{uav} + G_{ugv} - L_{FS(dB)}^{s1-2}, \tag{23}$$

where $L_{FS(dB)}^{s1-2}$ is the path loss between the UAV and the UGV given by (7) before. The final amount of energy that is available for charging can be derived as

$$E_{available}^{s1} = E_{uav-DC}^{s1} - E_{hover}^{s1} - E_{fly-to}^{s1} - E_{fly-back}^{s1}. \tag{24}$$

Note that, during the $charge$ stage the UAV also consumes energy with a power of P_{hover}^{s1} for hovering, similar to the $load$ stage (i.e. hovering consumption). Thus, the charging time in this stage can be calculated as:

$$T_{charging}^{s1} = \frac{E_{available}^{s1}}{10^{\frac{P_{uav-t}^{s1}}{10}} + P_{hover}}. \tag{25}$$

As a result, the energy that the UGV can receive is derived as

$$E_{ugv-DC}^{s1} = \eta E_{ugv\_RF}^{s1} = \eta 10^{\frac{P_{ugv}^{s1}}{10}} T_{charging}^{s1}. \tag{26}$$

Comparing (18) and (26), it can be seen that the conventional scheme is mainly affected by the transmission distance, while the proposed Scheme 1 is mainly affected by the UAV's own energy consumption and the RF-to-DC conversion (i.e. from the BS to the UAV and from the UAV to the UGV) efficiency. The proposed Scheme 1 saves energy by significantly reducing the transmission distance but has extra energy consumption due to hovering and flight operations. Thus, there might exist a trade-off between the transmission loss and the extra UAV operations. We will investigate this trade-off by finding the transmission distance beyond which the proposed Scheme 1 will have advantages over the conventional direct transfer.

To do this, we need to study the critical distance beyond which the cost of UAV-enabled WPT is lower than the transmission loss caused by path loss in the conventional direct transfer. Using (18) for the conventional direct transfer scheme, one has

$$E_{ugv-DC} = \frac{\eta T_{loading} 10^{\frac{P_t+G_t+G_{ugv}-20\lg\{f_c\}+147.55-X}{10}}}{10^{\frac{20\lg\left\{\sqrt{L^2+(H_t-H_r)^2}\right\}}{10}}} = \frac{\eta T_{loading} 10^{\frac{P_t+G_t+G_{ugv}-20\lg\{f_c\}+147.55-X}{10}}}{L^2+(H_t-H_r)^2}. \tag{27}$$

Since all parameters in (27) are constants except L, denote $A = T_{loading} 10^{\frac{P_t+G_t+G_{ugv}-20\lg\{f_c\}+147.55dB}{10}}$ and let $H = H_t - H_r$, one has

$$E_{ugv-DC} = \eta \frac{A}{L^2+H^2}. \tag{28}$$

Similarly, using (26) for the proposed Scheme 1, one has

$$E_{ugv-DC}^{s1} = \eta 10^{\frac{P_{ugv}^{s1}}{10}} \frac{E_{available}^{s1}}{10^{\frac{P_{uav-t}^{s1}}{10}} + P_{hover}}. \tag{29}$$

Denote $B = 10^{\frac{P_{ugv}^{s1}}{10}}$, $C = \eta 10^{\frac{P_{uav-r}^{s1}}{10}} T_{loading}^{s1} - E_{hover}^{s1} - 2\left(P_{\overline{acc}}^{s1}(\frac{v}{a}) + P_{dec}^{s1}(\frac{v}{a})\right)$, $D = 10^{\frac{P_{uav-t}^{s1}}{10}} + P_{hover}$, $E = \frac{2P_v}{v}$ and $F = \frac{v^2}{a}$. Then from (29), one has

$$E_{ugv-DC}^{s1} = \eta \frac{B}{D}\left(C - E\left(L - F\right)\right). \tag{30}$$

Using (28) and (30), the critical distance can be found by letting $E_{ugv-DC} = E^{s1}_{ugv-DC}$ and $T_{loading} = T^{s1}_{loading}$ (i.e. assuming that the energy released from the BS to UAV is fixed.) to give

$$\frac{A}{L^2+H^2} = \frac{B}{D}\left(C - E\left(L - F\right)\right). \tag{31}$$

It can be seen that (31) is an equation of the distance L only, and it can be solved by transforming it using the $Cardano$ formula. The solution to (31) can be found in Appendix A. This gives the two critical distances as

$$cd_1 = 2\sqrt[3]{\sqrt{-\left(\frac{p}{3}\right)^3}}\cos\left(\frac{1}{3}\arccos\left(-\frac{q}{2}\right) + 240^\circ\right), \tag{32}$$

and

$$cd_2 = 2\sqrt[3]{\sqrt{-\left(\frac{p}{3}\right)^3}}\cos\left(\frac{1}{3}\arccos\left(-\frac{q}{2}\right)\right) - \frac{b}{3a}. \tag{33}$$

where $cd_1 < cd_2$, $a = BE$, $b = -(BC + BEF)$, $c = BEH^2$, $d = -BCH^2 - BEFH^2 + AD$, $p = \frac{c}{a} - \frac{b}{3a^2}$, $q = \frac{2b^3}{27a^3} - \frac{bc}{3a^2} + \frac{d}{a}$, and A, B, C, D, E, F, H are defined as before. Accordingly, the critical range is derived as

$$cd_1 \leq critical\ range \leq cd_2. \tag{34}$$

2) The Proposed Scheme 2 in Fig. 3:

Now consider the proposed Scheme 2 in Fig. 3. In this scheme, instead of hovering above the BS in a static position for charging or discharging, the UAV starts at L_1 meters to the right of the BS and flies along both sides of the BS within a distance L_1 meters to be charged, and similarly within a distance of L_2 meters to be discharged. The main reason for this is that it is found that the hovering power P_{hover} is higher than the flying power P_v when the flying speed of v is relatively low [31] so that it may save more energy if the UAV stays mobile than staying static. The process of Scheme 2 in Fig. 3 can also be divided into three stages, $load$, $carry$ and $charge$.

a) Load: During this stage, within a horizontal distance of L_1 meters on both sides of the BS, the UAV is being charged. In order to ensure that the received power at the UAV is not too small or the amount is reasonable when the UAV is located at a horizontal distance of L_1 meters from the BS, we set a threshold of P_ϵ, so that the maximum value of L_1 when $P^{s2}_{uav-r} = P_\epsilon$ can be calculated according to

$$P^{s2}_{uav-r}(t) = P_t + G_t + G_{uav} - L^{s2-1}_{FS(dB)}(t) = P_\epsilon\ dB, \tag{35}$$

where $L^{s2-1}_{FS(dB)}(t)$ is the transmission loss from the BS to the UAV given in (10). The threshold of P_ϵ can be changed to any other value, depending on the application. Thus, the maximum L_1 can be derived as

$$L_1 = \sqrt{10^{\frac{P_t+G_t+G_{uav}-20\lg\{f_c\}+147.55-P_\epsilon}{10}} - {H_1}^2}, \tag{36}$$

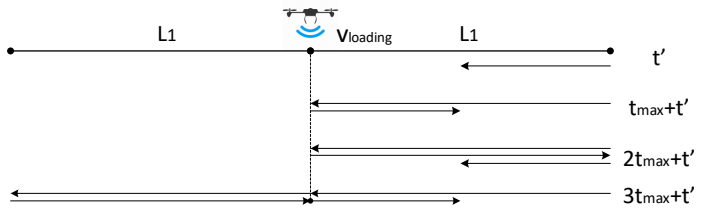

Fig. 4. Different loading cases (Scheme 2).

where $H_1 = H_{loading} - H_t$. Also, we assume that the UAV flies at a fixed speed of $v_{loading}$ during loading. The instantaneous distance between the UAV and the BS within a horizontal distance of L_1 meter is

$$d_{s2-1}(t) = \sqrt{{H_1}^2 + (L_1 - v_{loading}t)^2}, \tag{37}$$

where $L_1 \geq v_{loading}t$ so that $0 \leq t \leq \frac{L_1}{v_{loading}}$. Accordingly, the received instantaneous power at the UAV can be expressed as

$$P^{s2}_{uav-r}(t) = \Omega - 20\lg\left(d_{s2-1}(t)\right)\ dB. \tag{38}$$

Where $\Omega = P_t + G_t + G_{uav} - 20\lg(f_c) + 147.55$. Denote $t_{max} = \frac{L_1}{v_{loading}}$ as the maximum flight time on both sides of the BS. Since the received power at the UAV is changing with the time due to the flight, the total energy loaded during this time is

$$E_{t_{max}} = \eta 10^{\frac{\Omega}{10}} \int_0^{t_{max}} \frac{1}{{H_1}^2 + (L_1 - v_{loading}t)^2} dt = \eta 10^{\frac{\Omega}{10}} \left[\xi \tan^{-1}\frac{v_{loading}t_{max} - L_1}{H_1} - \xi \tan^{-1}\frac{-L_1}{H_1}\right], \tag{39}$$

where $\xi = \frac{1}{v_{loading}H_1}$, and we have used the integral in [43, eq. (2.103.4)]. It can be seen that the flight of the UAV is symmetric about the centre point right above the BS. In other words, the time that is taken to fly to the right or the left is the same and the total energy loaded is also the same. It takes four flights for the UAV to complete a cycle and go back to the starting position. Thus, the total energy loaded for a complete cycle is $4E_{t_{max}}$. Also, denote the total loading time as $T^{s2}_{loading}$, Thus, it takes $\left\lceil \frac{T^{s2}_{loading}}{t_{max}} \right\rceil$ flights to finish the energy loading. Several cases can be discussed as shown in Fig. 4.

In the first case, in addition to the full cycles, there is some time t' $(t' < t_{max})$ left due to an incomplete flight when the UAV flies towards the BS. We calculate the energy loaded within t' that is less than t_{max} as

$$E^{s2-1}_{t'} = \eta 10^{\frac{\Omega}{10}} \int_0^{t'} \frac{1}{{H_1}^2 + (L_1 - v_{loading}t)^2} dt = \eta 10^{\frac{\Omega}{10}} \left[\xi \tan^{-1}\frac{v_{loading}t' - L_1}{H_1} - \xi \tan^{-1}\frac{-L_1}{H_1}\right], \tag{40}$$

where $0 \leq t' < t_{max}$. In this case, denote the total number of full cycles as $n_{4t_{max}}$. Then , we can calculate the total energy loaded within $T^{s2}_{loading}$ as

$$E^{s2}_{uav-DC} = n_{4t_{max}} * 4E_{t_{max}} + E^{s2-1}_{t'}. \tag{41}$$

In the second case, there is $t_{max} + t'$ left due to one complete flight and one incomplete flight. For time t', since the UAV flies away from the BS, we calculate the energy loaded for this time as

$$E^{s2-2}_{t'} = \eta 10^{\frac{\Omega}{10}} \int_0^{t'} \frac{1}{{H_1}^2 + (v_{loading}t)^2} dt = \eta 10^{\frac{\Omega}{10}} \left[\frac{1}{v_{loading} H_1} tan^{-1} \left(t' \frac{v_{loading}}{H_1} \right) \right], \tag{42}$$

where we have also used the integral [43, eq. (2.103.4)] in (42) Thus, the total energy loaded in this case can be calculated as

$$E^{s2}_{uav-DC} = n_{4t_{max}} * 4E_{t_{max}} + E_{t_{max}} + E^{s2-2}_{t'}. \tag{43}$$

In the third case, there is $2t_{max}+t'$ left due to two complete flights and one incomplete flight. According to the Fig. 4, the total energy loaded in this case can be calculated as

$$E^{s2}_{uav-DC} = n_{4t_{max}} * 4E_{t_{max}} + 2E_{t_{max}} + E^{s2-1}_{t'}. \tag{44}$$

In the last case, there is $3t_{max} + t'$ left due to three complete flights and one incomplete flight. Thus, the total energy loaded in this case can be calculated as

$$E^{s2}_{uav-DC} = n_{4t_{max}} * 4E_{t_{max}} + 3E_{t_{max}} + E^{s2-2}_{t'}. \tag{45}$$

The following Algorithm 1 can be used to calculate the total energy loaded by the UAV during the first stage with a loading time of $T^{s2}_{loading}$ in different cases. Denote N as the total number of flights within $T^{s2}_{loading}$, $n_{4t_{max}}$ as the total number of full cycles and $n_{t_{max}}$ as the number of complete flights beyond the number of full cycles. Note that, during the $load$ stage the UAV also consumes energy for loading at a fixed speed of $v_{loading}$ with a power of $P_{v_{loading}}$ (watt). Thus, the consumption during $load$ stage can be derived as

$$E^{s2}_{v_{loading}} = P_{v_{loading}} T^{s2}_{loading}. \tag{46}$$

2) Carry: In this stage, after being charged by the BS in the above four different cases, an *acceleration-fly-deceleration* operation of the UAV will be performed to carry energy. Here is a summary of operations —the UAV starts to accelerate from $v_{loading}$ to a higher flight speed of v to deliver the energy. Then, it starts to decelerate from v to $v_{charging}$. As a result, the energy consumption of the $carry$ stage can be expressed as

$$E^{s2}_{fly-to} = \begin{cases} \Phi + P_{v_{loading}} t', \\ \Phi + P_{v_{loading}} \left(t_{max} - t' \right). \end{cases} \tag{47}$$

Algorithm 1 Calculate the total energy loaded within $T_{loading}^{s2}$

1: Calculate the total number of flights for a loading $N = \left\lfloor \frac{T_{loading}^{s2}}{t_{max}} \right\rfloor$ (floor function)
2: Calculate the number of full cycles during the loading process $n_{4t_{max}} = \left\lfloor \frac{N}{4} \right\rfloor$ (floor function). Each full cycle has four flights.
3: Exclude the number of flights during loading that does not make a full flight $t' = T_{loading}^{s2} - N * t_{max}$.
4: The total energy loaded during $T_{loading}^{s2}$ can be calculated as:
5: **if** $n_{t_{max}} = 0$ or $n_{t_{max}} = 2$ **then**
6: $E_{uav-DC}^{s2} = n_{4t_{max}} * E_{4t_{max}} + n_{t_{max}} * E_{t_{max}} + E_{t'}^{s2-1}$
7: **else if** $n_{t_{max}} = 1$ or $n_{t_{max}} = 3$ **then**
8: $E_{uav-DC}^{s2} = n_{4t_{max}} * E_{4t_{max}} + n_{t_{max}} * E_{t_{max}} + E_{t'}^{s2-2}$
9: **end if**

Where $\Phi = P_{\overline{acc}}^{s2}\left(\frac{v-v_{loading}}{a}\right) + P_{\overline{dec}}^{s2}\left(\frac{v-v_{charging}}{a}\right) + P_v^{s2}\frac{\left(L-(L_1+L_2)-\frac{v^2-{v_{loading}}^2}{a}\right)}{v}$ and $L-(L_1+L_2)-\frac{v^2-{v_{loading}}^2}{a} > 0$. Otherwise, there is no *carry* stage, similar to what discussed in (22), $P_{v_{loading}}t'$ and $P_{v_{loading}}\left(t_{max}-t'\right)$ in (47) are the consumption during the rest of the $load$ stage caused by incomplete flights when $n_{t_{max}} = 0, 2$ and $n_{t_{max}} = 1, 3$ respectively.

3) Charge: In the third stage, we firstly derived the received RF power at the UGV as

$$P_{ugv}^{s2} = P_{uav-t}^{s2} + G_{uav} + G_{ugv} - L_{FS(dB)}^{s2-2}\left(t\right), \tag{48}$$

where $L_{FS(dB)}^{s2-2}\left(t\right)$ is the transmission loss from the UAV to the UGV given in (11). And the instantaneous distance in this case is given as

$$d_{s2-2}\left(t\right) = \sqrt{{H_2}^2 + \left(L_2 - v_{charging}t\right)^2}, \tag{49}$$

where $H_2 = H_{charging} - H_r$, $H_{charging} > H_r$, $L_2 \geq v_{loading}t$ so that $0 \leq t \leq \frac{L_2}{v_{loading}}$, L_2 is the maximum distance when $t = 0$ by letting $P_{ugv}^{s2} = -33\ dBm$ to give

$$L_2 = \sqrt{10^{\frac{\Omega'-16}{10}} - {H_2}^2}. \tag{50}$$

Where $\Omega' = P_{uav-t}^{s2} + G_{uav} + G_{ugv} - 20\lg\left(f_c\right) + 147.55$. Hence, the received instantaneous power at the UGV can be expressed as

$$P_{ugv}^{s2}\left(t\right) = \Omega' - 20\lg\left(d_{s2-2}\left(t\right)\right). \tag{51}$$

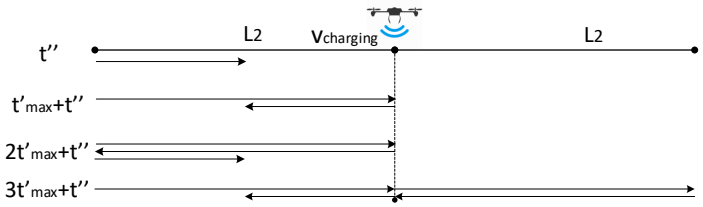

Fig. 5. Different charging cases (Scheme 2).

Similar to the $load$ stage, denote the $t'_{max} = \frac{L_2}{v_{charging}}$ as the maximum flight time on both sides of the UGV. Since the received power at the UGV is changing with the time because of the flight. the total energy received at the UGV during this time is

$$E_{t'_{max}} = \eta 10^{\frac{\Omega'}{10}} \int_0^{t'_{max}} \frac{1}{H_2^2+(L_2-v_{charging}t)^2} dt = \eta 10^{\frac{\Omega'}{10}} \left[\xi' \tan^{-1} \frac{v_{charging}t'_{max}-L_2}{H_2} - \xi' \tan^{-1} \frac{-L_2}{H_2}\right] \quad (52)$$

where $\xi' = \frac{1}{v_{charging}H_2}$ and [43, eq. (2.103.4)] is used here again. Note that, in order to make sure that the UAV can fly back to its initial position, the energy consumption for flying back, which is denoted as $E^{s2}_{fly-back}$, need to be considered. Then, $E^{s2}_{fly-back}$ can be calculated as

$$E^{s2}_{fly-to} = \begin{cases} \Phi' + P_{v_{charging}} t'', \\ \Phi' + P_{v_{charging}} \left(t'_{max} - t''\right), \end{cases} \quad (53)$$

where $\Phi' = P^{s2}_{\overline{acc}} \left(\frac{v-v_{charging}}{a}\right) + P^{s2}_{\overline{dec}} \left(\frac{v-v_{loading}}{a}\right) + P^{s2}_{v} \frac{\left(L-(L_1+L_2)-\frac{v^2-{v_{charging}}^2}{a}\right)}{v}$, $L-(L_1+L_2)-\frac{v^2-{v_{charging}}^2}{a} > 0$, $P_{v_{charging}} t''$ and $P_{v_{charging}}(t'_{max}-t'')$ in (53) are the power consumption during the rest of the $charge$ stage due to incomplete flights when $n_{t'_{max}} = 0, 2$ and $n_{t'_{max}} = 1, 3$, respectively. However, it is difficult to calculate $E^{s2}_{fly-back}$ without knowing t'', because t'' is derived from $E^{s2}_{available}$ which is derived assuming knowledge of $E^{s2}_{fly-back}$. Thus, for convenience and in order to make sure the UAV has enough energy for flying back, the upper bound time t'_{max} is used, i.e. $P_{v_{charging}} t'_{max}$, to calculate the power consumption in the rest of the $charge$ stage in Section IV. Consequently, the available energy for $charging$ can be derived as

$$E^{s2}_{available} = E^{s2}_{uav-DC} - E^{s2}_{vloading} - E^{s2}_{fly-to} - E^{s2}_{fly-back}. \quad (54)$$

Fig. 5 shows different charging cases. It can be also seen that the flight of the UAV is symmetric about the centre point right above the UGV. Thus, the time taken to fly to the right or the left is the same and the total energy to be charged is the same as well. It takes four flights for the UAV to complete a cycle

and go back to the initial position. Therefore, the total energy received at the UGV for a complete cycle is $4E_{t'_{max}}$. Denote the total charging time as $T^{s2}_{charging}$ and in this case it can be calculated as

$$T^{s2}_{charing} = \frac{E^{s2}_{available}}{10\frac{P^{s2}_{uav-t}}{10} + P_{v_{charging}}}. \tag{55}$$

Thus, it takes $\left\lceil \frac{T^{s2}_{charging}}{t'_{max}} \right\rceil$ flights to finish the energy discharging. Several cases in Fig. 5 can be discussed.

In the first case, there is only t'' ($t'' < t'_{max}$) seconds left for an incomplete flight when the UAV flies towards the UGV. The energy received at the UGV during t'' is

$$E^{s2-3}_{t''} = \eta 10^{\frac{\Omega'}{10}} \int_0^{t''} \frac{1}{H_2^2 + (L_2 - v_{charging}t)^2} dt = \eta 10^{\frac{\Omega'}{10}} \left[\xi' \tan^{-1} \frac{v_{charging}t'' - L_2}{H_2} - \xi' \tan^{-1} \frac{-L_2}{H_2} \right], \tag{56}$$

where $H_2 = H_{charging} - H_r$ and $0 \leq t'' < t'_{max}$. Denote the total number of full cycles as $n_{4t'_{max}}$. Then, we can calculate the total energy discharged during $T^2_{charging}$ as

$$E^{s2}_{ugv-DC} = n_{4t'_{max}} * 4E_{t'_{max}} + E^{s2-3}_{t''}. \tag{57}$$

In the second case, there is $t'_{max} + t''$ left due to one complete flight and one incomplete flight. For time t'', since the UAV flies away from the UGV, we calculate the energy discharged during t'' as

$$E^{s2-4}_{t''} = \eta 10^{\frac{\Omega'}{10}} \int_0^{t''} \frac{1}{{H_2}^2 + (v_{charging}t)^2} dt = \eta 10^{\frac{\Omega'}{10}} \left[\xi' \tan^{-1} \left(t'' \frac{v_{charging}}{H_2} \right) \right], \tag{58}$$

where $0 \leq t'' < t'_{max}$. In this case, the total energy discharged can be calculated as

$$E^{s2}_{ugv-DC} = n_{4t'_{max}} * 4E_{t'_{max}} + E_{t'_{max}} + E^{s2-4}_{t''}. \tag{59}$$

In the third case, there is $2t'_{max} + t''$ left due to two complete flights and one incomplete flight. According to Fig. 5, the total energy discharged in this case can be calculated as

$$E^{s2}_{ugv-DC} = n_{4t'_{max}} * 4E_{t'_{max}} + 2E_{t'_{max}} + E^{s2-3}_{t''}. \tag{60}$$

In the last case, if there is $3t'_{max} + t''$ left due to three complete flights and one incomplete flight, Thus, the total energy discharged in this case can be calculated as

$$E^{s2}_{ugv-DC} = n_{4t'_{max}} * 4E_{t'_{max}} + 3E_{t'_{max}} + E^{s2-4}_{t''}. \tag{61}$$

Algorithm 2 can be used to calculate the total energy received by the UGV during the $charge$ stage within time $T^{s2}_{charging}$. Denote N' as the total number of flights within $T^{s2}_{charging}$, $n_{4t'_{max}}$ as the total number of full cycles and $n_{t'_{max}}$ as the number of complete flights beyond the number of full cycles.

Algorithm 2 Calculate the total energy charged within $T_{charging}^{s2}$

1: Calculate the total number of flights for charging process $N' = \left\lfloor \frac{T_{charging}^{s2}}{t'_{max}} \right\rfloor$ (floor function)
2: Calculate the number of full cycles during charging process $n_{4t'_{max}} = \left\lfloor \frac{N'}{4} \right\rfloor$ (floor function). Each full cycle has four flights.
3: Exclude the number of flights during charging that does not make a full cycle $t'' = T_{charging}^{s2} - N' * t'_{max}$
4: The total energy charged within $T_{charging}^{s2}$ can be calculated as
5: **if** $n_{t'_{max}} = 0$ or $n_{t'_{max}} = 2$ **then**
6: $E_{ugv-DC}^{s2} = n_{4t'_{max}} * E_{4t'_{max}} + n_{t'_{max}} * E_{t'_{max}} + E_{t''}^{s2-3}$
7: **else if** $n_{t'_{max}} = 1$ or $n_{t'_{max}} = 3$ **then**
8: $E_{ugv-DC}^{s2} = n_{4t'_{max}} * E_{4t'_{max}} + n_{t'_{max}} * E_{t'_{max}} + E_{t''}^{s2-4}$
9: **end if**

Next, We will investigate the trade-off by finding the transmission critical distance beyond which the proposed Scheme 2 has advantages over the conventional direct transfer. According to Algorithm 2, the total energy harvested by the UGV with $T_{charging}^{s2}$ can be expressed as

$$\begin{aligned} E_{ugv-DC}^{s2} = &\left\lfloor \frac{\lfloor \Psi \rfloor}{4} \right\rfloor * E_{4t'_{max}} + (\lfloor \Psi \rfloor \bmod 4) * E_{t'_{max}} + ((((\lfloor \Psi \rfloor \bmod 4) + 1) \bmod 2) * E_{t''}^{s2-3} \\ &+ ((\lfloor \Psi \rfloor \bmod 4) \bmod 2) * E_{t''}^{s2-4}, \end{aligned} \tag{62}$$

where $\Psi = \frac{T_{charging}^{s2}}{t'_{max}}$. Using (28) and (62) (i.e.$E_{ugv-DC} = E_{ugv-DC}^{s2}$), we have

$$\begin{aligned} \eta \frac{A}{L^2 + H^2} = &\left\lfloor \frac{\lfloor \Psi \rfloor}{4} \right\rfloor * E_{4t'_{max}} + (\lfloor \Psi \rfloor \bmod 4) * E_{t'_{max}} + ((((\lfloor \Psi \rfloor \bmod 4) + 1) \bmod 2) * E_{t''}^{s2-3} \\ &+ ((\lfloor \Psi \rfloor \bmod 4) \bmod 2) * E_{t''}^{s2-4}. \end{aligned} \tag{63}$$

It is not easy to solve the above equation. The critical distance in Scheme 2 can be obtained numerically. We next consider the more general case when multiple UGVs are charged.

C. Conventional Scheme with Multiple UGVs

In this case, n UGVs need to be powered. Assume that these UGVs are very close to each other so that their distances to the BS are approximately the same. Then, the total energy harvested by n UGVs in this case can be calculated as

$$E_{ugvs-DC} = \sum_{i=1}^{n} E_{ugv_i-DC} = \sum_{i=1}^{n} \eta 10^{\frac{P_{ugv_i}}{10}} T_{loading}, \tag{64}$$

where $i = 1, 2, ..., n$ index different UGVs, P_{ugv_i} is the received power of the i-th UGV, $E_{ugv_i\_RF}$ is the received RF energy of the i-th UGV and E_{ugv_i-DC} is the converted DC energy of the i-th UGV. One has

$$P_{ugv_i} = \ P_t + G_t + G_{ugv_i} - 20\text{lg}\left\{f_c\right\} - 20\text{lg}\left\{d_0\right\} + 147.55 - X \ dB, \tag{65}$$

$$E_{ugv_i\_RF} = 10^{\frac{P_{ugv_i}}{10}} T_{loading}, \tag{66}$$

$$E_{ugv_i\_DC} = \eta E_{ugv_i\_RF}. \tag{67}$$

D. The Proposed Schemes with Multiple UGVs

Similar to the above case, there are n UGVs in this case. They are approximately of the same distance to the UAV. For the proposed Scheme 1, the total energy harvested by n UGVs can be derived from (26) as:

$$E^{s1}_{ugvs-DC} = \sum_{i=1}^{n} E^{s1}_{ugv_i-DC} = \sum_{i=1}^{n} \eta 10^{\frac{P^{s1}_{ugv_i}}{10}} T^{s1}_{charging}, \tag{68}$$

where $i = 1, 2, ..., n$ index different UGVs. For the proposed Scheme 2, the total energy harvested by n UGVs can be derived based on Algorithm 2 as

$$\begin{aligned} E^{s2}_{ugvs-DC} = \sum_{i=1}^{n} \left\lfloor \frac{\lfloor \Psi \rfloor}{4} \right\rfloor * E_{4t'_{max}} + (\lfloor \Psi \rfloor \bmod 4) * E_{t'_{max}} + (((\lfloor \Psi \rfloor \bmod 4) + 1) \bmod 2) * E^{s2-3}_{t''} \\ + ((\lfloor \Psi \rfloor \bmod 4) \bmod 2) * E^{s2-4}_{t''}. \end{aligned} \tag{69}$$

It is noted that the case when multiple UGVs are not close to each other is an interesting issue for future works. Since this issue will lead to many optimization problems, such as optimal hovering position, trajectory design and power optimization, etc., it is beyond the scope of this work.

IV. Numerical Results and Discussion

In this section, numerical examples are presented to show the energy performances of the proposed schemes. First, we compare the conventional scheme and the proposed schemes for a single UGV. Then, we expand the discussion to the case of multiple UGVs. In the comparison, we set $P_t = 35.68 \ dBw$, $G_t = 15 \ dBi$ [44], $G_{uav} = 2 \ dBi$, $G_{ugv} = 5 \ dBi$, $P^{s1}_{uav-t} = P^{s2}_{uav-t} = 40 \ dBm$, $H_{loading} = 6 \ m$ $H_t = 5 \ m$, $H_r = 0.5 \ m$, $f_c = 915$ MHZ, $T_{loading} = T^{s1}_{loading} = T^{s2}_{loading} = 1200 \ s$, $P_{hover} = 32.65 \ W$, $P_v = P^{s1}_v = P^{s2}_v = 20 \ W$, $P^{s1}_{acc} = P^{s1}_{dec} = P^{s2}_{acc} = P^{s2}_{dec} = 28 \ W$, $V = 10 \ m/s$, $a = 1 \ m/s^2$, $X = 18 \ dB$ and the RF-to-DC conversion efficiency $\eta = 0.6$, if not stated otherwise. Our expressions are general enough for arbitrary parameters and hence, these values are only used for illustration purpose. The value of the distance L is set from $100 \ m$ to $1600 \ m$ with a step size of $25 \ m$.

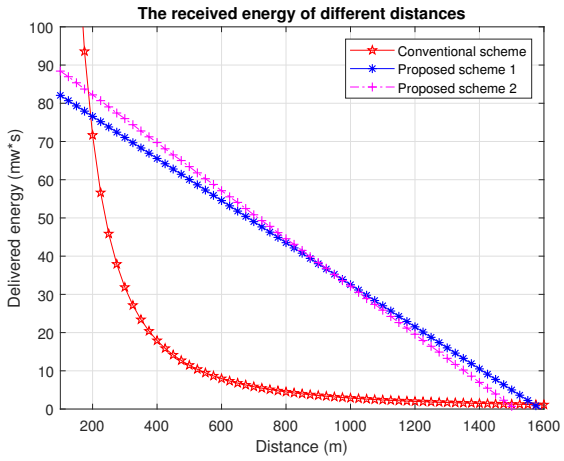

Fig. 6. The comparison of the proposed Scheme 1 and Scheme 2.

Fig. 6 shows the amount of the received energy at the UGV versus distance L. Firstly, we consider the proposed Scheme1. One can see that, when the total energy transmitted by the BS is fixed, the energy received by the UGV decreases with the distance in both the conventional scheme and the proposed Scheme 1 because of the path loss and UAV internal loss. However, as seen in Fig. 6, the total energy obtained in the conventional scheme decreases exponentially with the transmission distance. This is due to the fact that the path loss is a logarithmic function of transmission distance. Beyond a transmission distance of about $1500\ m$, the received energy is very close to 0. On the other hand, the straight line with asterisks representing the proposed Scheme 1 shows that its received energy decreases linearly with a fixed slope and hence is a linear function of the transmission distance. Thus, UAV-enabled WPT can improve the energy transfer efficiency greatly. As shown in Fig. 6, there are two intersection points between the conventional scheme and the proposed Scheme 1. The corresponding X coordinate is the critical distance, which is $[192.99\ m \quad 1569.62\ m]$ in this case derived from (32) and (33). Thus, when the transmission distance is within this range, the proposed Scheme 1 shows superiority over the conventional direct transfer scheme.

Next, we investigate the proposed Scheme 2. In this case, we set $P_{v_{loading}} = 25.5$ W, and the minimum value of P_{uav-r}^{s2} is set to 21 dBW (i.e. $P_{\epsilon} = 21\ dBW$). Fig. 6 also compares the conventional scheme and the proposed Scheme 2 represented by the straight line with plus signs. Similar observations can be made. Again, the received energy in the conventional scheme decreases exponentially with the distance, while it decreases linearly in the proposed Scheme 2. Also, compared with the Scheme 1, we can see that the energy loaded from the BS of Scheme 2 is higher than that of Scheme 1. For Scheme 1, the UAV hovers over the BS during loading. Although the path loss between the UAV and the BS is minimum and

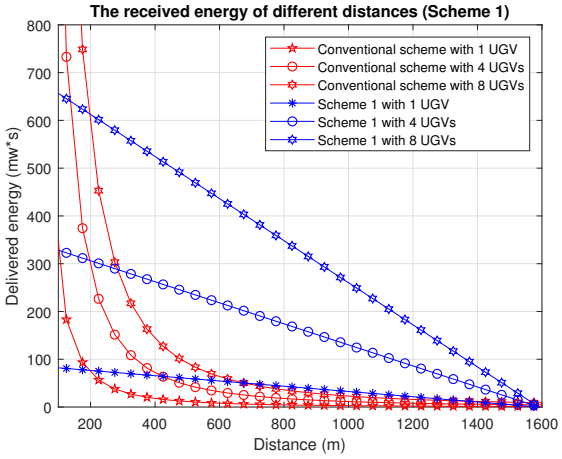

Fig. 7. Comparison of the conventional scheme and the proposed Scheme 1 with multiple UGVs. (The number is 1, 4 and 8 respectively.)

remains unchanged, it consumes larger energy to keep hovering with a power of P_{hover}. For Scheme 2, the UAV no longer hovers over the BS with a power of P_{hover}, but flies around the BS during loading with at a fixed speed of $V_{loading}$, which means it suffers from larger path loss with longer distance. The path loss becomes larger when the UAV flies farther away from the BS. Although the distance between the UAV and the BS changes with time and in general is larger than that in Scheme 1, the propulsion power of $P_{v_{loading}}$ is smaller than P_{hover}. From Fig. 6, we can see that the critical range of Scheme 2 is between $188\ m$ and $1490\ m$. This critical distance is smaller than that in Scheme 1.

From Fig.6, one can see that the critical range in Scheme 1 is between $192.99\ m$ and $1569.62\ m$, and that in Scheme 2 is between $188\ m$ and $1490\ m$. The range in Scheme 2 is smaller than that in Scheme 1, which means the Scheme 2 has advantages than Scheme 1 by having shorter distances. As shown in this figure, there is one intersection point between Scheme 1 and Scheme 2. The corresponding X coordinate value is about $942\ m$, beyond which Scheme 1 has better efficiency than Scheme 2. This is due to the fact that, although the energy loaded by the UAV in Scheme 2 from the BS during $load$ stage is larger than that of Scheme 1 since the $P_{v_{loading}}$ is small than P_{hover}, it suffers from an even larger path loss during the $charge$ stage. Although the UAV in Scheme 1 suffers from an even larger consumption of hovering in these two stages. the path loss between the UAV and the UGV is minimum and remains unchanged. Next, we will examine the effects of different system parameters on the critical range.

Fig. 7 uses the proposed Scheme 1 as an example to compare the conventional scheme and the proposed Scheme 1 for multiple UGVs. We set the number of the UGVs to 1, 4 and 8 using (64) and (68). As

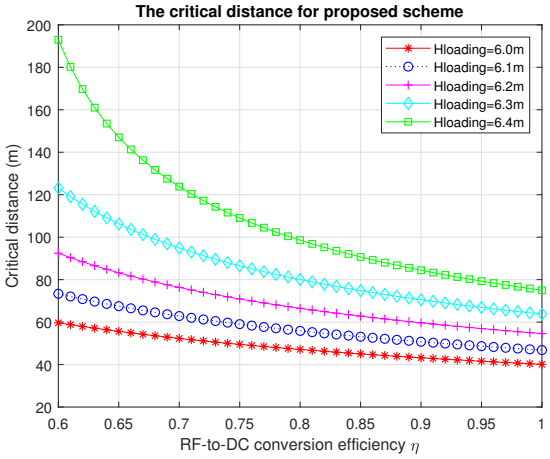

Fig. 8. The effects of RF-to-DC conversion efficiency η on the proposed scheme 1 performance for different flight heights.

shown in this figure, the curves in Fig. 7 have exactly the same trend as those in Fig. 6, except that the rate of decrease is proportional to the number of UGVs. There are six intersection points in the figure. Note that the critical range observed in Fig. 6 remains the same in this figure, as all the parameters are the same except for the number of UGVs but this number does not change the intersection points.

Fig. 8 examines the effect of the RF-to-DC conversion efficiency η on the critical distance. First, one can see that the critical distance decreases with η. This is because a higher conversion efficiency leads to more loaded or charged energy and hence, gives the proposed Scheme 1 more advantages with a shorter critical distance. It can also be seen that the higher the flight altitude is, the greater the critical distance will be. In these curves, we consider the starting point of the critical range. When the transmission distance exceeds this critical distance without exceeding the critical range, the Scheme 1 shows better energy transfer efficiency performance. The same performance can also be seen for Scheme 2.

Fig. 9 examines the effect of the flight height on the critical distance. The height of the BS is assumed to be $5\ m$, and the height of the UGV is set as $0.5\ m$. First, one can see that the critical distance increases with the flight height of loading. This is because a lower height of loading leads to more loaded or charged energy and thus, gives the proposed Scheme 1 and Scheme 2 more advantages with a shorter critical distance. When the loading height increases, the path loss increases. As a result, the energy obtained by the UAV is reduced, which is unfavourable to the proposed schemes. Note that, the conventional direct transfer scheme is the existing algorithm. There is no other energy ferry work in the literature.

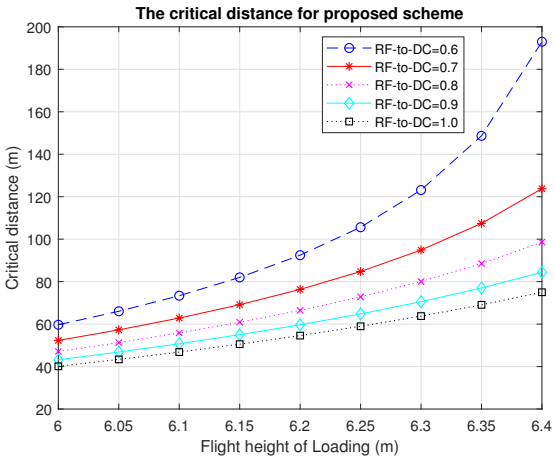

Fig. 9. The effects of the loading height of the UAV on the proposed Scheme 1 performance for different RF-to-DC conversion efficiency η.

V. Conclusion

In this paper, we have studied the WPT efficiency in UAV-enabled wireless networks. We have proposed two schemes for UAV-enabled WPT. By solving the energy equations, critical ranges have been derived. Numerical results have shown that the energy received by the UGV decreases with the transmission distance because of the path loss and UAV internal loss in both schemes. Within the critical range, the proposed two schemes have been shown to have better performances than the conventional scheme. The lower the loading height or the larger the RF-to-DC conversion efficiency is, the smaller the critical distance will be. To improve the performance of the proposed schemes further, one needs to carefully adjust parameters, such as task time, antenna gain, transmit power, energy conversion efficiency, battery capacity on the UAV, and the UAV velocity, which could require optimization with extra costs.

Appendix A Solution to (31)

In this appendix, we solve the equation to derive the exact critical range in which it shows the superiority for the proposed Scheme 1. Rewriting equation (31), we can transform it into a standard form of a cubic equation as below:

$$BEL^3 - (BC + BEF)\,L^2 + BEH^2L - BCH^2 - BEFH^2 + AD = 0 \tag{70}$$

Because A, B, C, D, E and B are constants, (70) can be derived in an easier form via the constant transformation $a = BE$, $b = -(BC + BEF)$, $c = BEH^2$ and $d = -BCH^2 - BEFH^2 + AD$.

$$aL^3 + bL^2 + cL + d = 0 \tag{71}$$

For (71), we divide both sides of the equation by a simultaneously, and then it can be transformed into the form of $Cardano$ formula using the variable transformation $L = y - \frac{b}{3a}$ as

$$y^3 + \left(\frac{c}{a} - \frac{b^2}{3a^2}\right) y + \left(\frac{2b^3}{27a^3} - \frac{bc}{3a^2} + \frac{d}{a}\right) = 0. \tag{72}$$

Accordingly, the discriminant of the equation root can be expressed via variable transformation $p = \frac{c}{a} - \frac{b}{3a^2}$ and $q = \frac{2b^3}{27a^3} - \frac{bc}{3a^2} + \frac{d}{a}$ as

$$\Delta = \left(\frac{q}{2}\right)^2 + \left(\frac{p}{3}\right)^3 \tag{73}$$

It is not difficult to find that $\Delta < 0$ and $p < 0$ in this case. Therefore, three unequal real roots of the equation (72) can be obtained according to the $Cardano$ formula as

$$\begin{aligned} y_1 &= 2\sqrt[3]{r}\cos\theta; \\ y_2 &= 2\sqrt[3]{r}\cos\left(\theta + 120^\circ\right); \\ y_3 &= 2\sqrt[3]{r}\cos\left(\theta + 240^\circ\right). \end{aligned} \tag{74}$$

where,

$$r = \sqrt{-\left(\frac{p}{3}\right)^3}, \theta = \frac{1}{3}\arccos\left(-\frac{q}{2}\right) \tag{75}$$

Consequently, the three real roots of the equation (71) are

$$\begin{aligned} L_1 &= y_1 - \frac{b}{3a}; \\ L_2 &= y_2 - \frac{b}{3a}; \\ L_3 &= y_3 - \frac{b}{3a}. \end{aligned} \tag{76}$$

And the final solutions of the equation (71) after reorganizing are

$$\begin{aligned} L_1 &= 2\sqrt[3]{\sqrt{-\left(\frac{p}{3}\right)^3}}\cos\left(\frac{1}{3}\arccos\left(-\frac{q}{2}\right)\right) - \frac{b}{3a}; \\ L_2 &= 2\sqrt[3]{\sqrt{-\left(\frac{p}{3}\right)^3}}\cos\left(\frac{1}{3}\arccos\left(-\frac{q}{2}\right) + 120^\circ\right) - \frac{b}{3a}; \\ L_3 &= 2\sqrt[3]{\sqrt{-\left(\frac{p}{3}\right)^3}}\cos\left(\frac{1}{3}\arccos\left(-\frac{q}{2}\right) + 240^\circ\right) - \frac{b}{3a}. \end{aligned} \tag{77}$$

By substituting the values of the parameters for simulation, we can find that L_2 is a negative value among the above three roots, which is obviously meaningless in our model because L is a positive number. While L_3 and L_1 are the two values on both the left and right sides of the critical rang $[L_3 \quad L_1]$ we expect, and L_3 is seen as the critical distance.

REFERENCES

[1] S. Hayat, E. Yanmaz, and R. Muzaffar, "Survey on Unmanned Aerial Vehicle Networks for Civil Applications: A Communications Viewpoint," *IEEE Commun. Surv. Tutorials*, vol. 18, no. 4, pp. 2624–2661, 2016.

[2] Y. Zeng, R. Zhang, and T. J. Lim, "Wireless communications with unmanned aerial vehicles: opportunities and challenges," *IEEE Commun. Mag.*, vol. 54, no. 5, pp. 36–42, May 2016.

[3] L. Gupta, R. Jain, and G. Vaszkun, "Survey of Important Issues in UAV Communication Networks," *IEEE Commun. Surv. Tutorials*, vol. 18, no. 2, pp. 1123–1152, 2016.

[4] A. Al-Hourani, S. Kandeepan, and S. Lardner, "Optimal LAP Altitude for Maximum Coverage," *IEEE Wirel. Commun. Lett.*, vol. 3, no. 6, pp. 569–572, Dec. 2014.

[5] Y. Chen, W. Feng, and G. Zheng, "Optimum Placement of UAV as Relays," *IEEE Commun. Lett.*, vol. 22, no. 2, pp. 248–251, Feb. 2018.

[6] Y. Zeng, R. Zhang, and T. J. Lim, "Throughput Maximization for UAV-Enabled Mobile Relaying Systems," *IEEE Trans. Commun.*, vol. 64, no. 12, pp. 4983–4996, Dec. 2016.

[7] J. Lyu, Y. Zeng, R. Zhang, and T. J. Lim, "Placement Optimization of UAV-Mounted Mobile Base Stations," *IEEE Commun. Lett.*, vol. 21, no. 3, pp. 604–607, Mar. 2017.

[8] J. Lyu, Y. Zeng, and R. Zhang, "Cyclical Multiple Access in UAV-Aided Communications: A Throughput-Delay Tradeoff," *IEEE Wirel. Commun. Lett.*, vol. 5, no. 6, pp. 600–603, Dec. 2016.

[9] R. Fan, J. Cui, S. Jin, K. Yang, and J. An, "Optimal Node Placement and Resource Allocation for UAV Relaying Network," *IEEE Commun. Lett.*, pp. 1–1, 2018.

[10] S. Zhang, H. Zhang, Q. He, K. Bian, and L. Song, "Joint Trajectory and Power Optimization for UAV Relay Networks" *IEEE Commun. Lett.*, vol. 22, no. 1, pp. 161–164, Jan. 2018.

[11] J. Xu, Y. Zeng, and R. Zhang, "UAV-Enabled Wireless Power Transfer: Trajectory Design and Energy Region Characterization," in *2017 IEEE Globecom Workshops (GC Wkshps)*, 2017, pp. 1–7.

[12] J. Xu, Y. Zeng, and R. Zhang, "UAV-enabled multiuser wireless power transfer: Trajectory design and energy optimization," in *2017 23rd Asia-Pacific Conference on Communications (APCC)*, 2017, pp. 1–6.

[13] J. Xu, Y. Zeng, and R. Zhang, "UAV-Enabled Wireless Power Transfer: Trajectory Design and Energy Optimization," *IEEE Trans. Wirel. Commun.*, vol. 17, no. 8, pp. 5092–5106, Aug. 2018.

[14] Y. Hu, X. Yuan, J. Xu, and A. Schmeink, "Optimal 1D Trajectory Design for UAV-Enabled Multiuser Wireless Power Transfer," Nov. 2018. [Online]. Available: https://arxiv.org/abs/1811.00471

[15] Y. Wu, L. Qiu, and J. Xu, "UAV-Enabled Wireless Power Transfer with Directional Antenna: A Two-User Case (Invited Paper)," in 2018 15th International Symposium on Wireless Communication Systems (ISWCS), 2018, pp. 1–6.

[16] Q. Wu, Y. Zeng, and R. Zhang, "Joint Trajectory and Communication Design for Multi-UAV Enabled Wireless Networks," *IEEE Trans. Wirel. Commun.*, vol. 17, no. 3, pp. 2109–2121, Mar. 2018.

[17] M. Hua, C. Li, Y. Huang, and L. Yang, "Throughput maximization for UAV-enabled wireless power transfer in relaying system," in *2017 9th International Conference on Wireless Communications and Signal Processing (WCSP)*, 2017, pp. 1–5.

[18] D. Yang, Q. Wu, Y. Zeng, and R. Zhang, "Energy Trade-off in Ground-to-UAV Communication via Trajectory Design," *IEEE Trans. Veh. Technol.*, pp. 1–1, 2018.

[19] H. J. Visser and R. J. M. Vullers, "RF Energy Harvesting and Transport for Wireless Sensor Network Applications: Principles and Requirements," *Proc. IEEE*, vol. 101, no. 6, pp. 1410–1423, Jun. 2013.

[20] Liguang Xie, Yi Shi, Y. T. Hou, and A. Lou, "Wireless power transfer and applications to sensor networks," *IEEE Wirel. Commun.*, vol. 20, no. 4, pp. 140–145, Aug. 2013.

[21] X. Lu, P. Wang, D. Niyato, D. I. Kim, and Z. Han, "Wireless Networks With RF Energy Harvesting: A Contemporary Survey," *IEEE Commun. Surv. Tutorials*, vol. 17, no. 2, pp. 757–789, 2015.

[22] D. Mishra, S. De, S. Jana, S. Basagni, K. Chowdhury, and W. Heinzelman, "Smart RF energy harvesting communications: challenges and opportunities," *IEEE Commun. Mag.*, vol. 53, no. 4, pp. 70–78, Apr. 2015.

[23] X. Lu, P. Wang, D. Niyato, D. I. Kim, and Z. Han, "Wireless Charging Technologies: Fundamentals, Standards, and Network Applications," *IEEE Commun. Surv. Tutorials*, vol. 18, no. 2, pp. 1413–1452, 2016.

[24] M. Lu, M. Bagheri, A. P. James, and T. Phung, "Wireless Charging Techniques for UAVs: A Review, Reconceptualization, and Extension," *IEEE Access*, pp. 1–1, 2018.

[25] M. Y. Naderi, K. R. Chowdhury, and S. Basagni, "Wireless sensor networks with RF energy harvesting: Energy models and analysis," in *2015 IEEE Wireless Communications and Networking Conference (WCNC)*, 2015, pp. 1494–1499.

[26] S. Kumar, S. De, and D. Mishra, "RF Energy Transfer Channel Models for Sustainable IoT," *IEEE Internet Things J.*, pp. 1–1, 2018.

[27] F. Sangare, A. Arab, Miao Pan, Lijun Qian, S. K. Khator, and Zhu Han, "RF energy harvesting for WSNs via dynamic control of unmanned vehicle charging," in *2015 IEEE Wireless Communications and Networking Conference (WCNC)*, 2015, pp. 1291–1296.

[28] F. Sangare, Y. Xiao, D. Niyato, and Z. Han, "Mobile Charging in Wireless-Powered Sensor Networks: Optimal Scheduling and Experimental Implementation," *IEEE Trans. Veh. Technol.*, vol. 66, no. 8, pp. 7400–7410, Aug. 2017.

[29] W. Na et al., "Energy-Efficient Mobile Charging for Wireless Power Transfer in Internet of Things Networks," *IEEE Internet Things J.*, pp. 1–1, 2017.

[30] N. Zhao, F. R. Yu, and V. C. M. Leung,"Wireless energy harvesting in interference alignment networks," *IEEE Commun. Mag.*, vol. 53, no. 6, pp. 72–78, Jun. 2015.

[31] Y. Zeng, J. Xu, R. Zhang, Y. Zeng, R. Zhang, and J. Xu, "Energy Minimization for Wireless Communication with Rotary-Wing UAV", 2018.

[32] S. Suman, S. Kumar, and S. De, "UAV-Assisted RF Energy Transfer," *2018 IEEE International Conference on Communications (ICC)*, 2018, pp. 1–6.

[33] C.-M. Cheng, P.-H. Hsiao, H. T. Kung, and D. Vlah, "Maximizing Throughput of UAV-Relaying Networks with the Load-Carry-and-Deliver Paradigm," in *2007 IEEE Wireless Communications and Networking Conference*, 2007, pp. 4417–4424.

[34] C. Li, S. Zhang, P. Liu, F. Sun, J. M. Cioffi, and L. Yang, "Overhearing Protocol Design Exploiting Intercell Interference in Cooperative Green Networks," *IEEE Trans. Veh. Technol.*, vol. 65, no. 1, pp. 441–446, Jan. 2016.

[35] C. Li, H. J. Yang, F. Sun, J. M. Cioffi, and L. Yang, "Multiuser Overhearing for Cooperative Two-Way Multiantenna Relays," *IEEE Trans. Veh. Technol.*, vol. 65, no. 5, pp. 3796–3802, May 2016.

[36] C. Li, P. Liu, C. Zou, F. Sun, J. M. Cioffi, and L. Yang, "Spectral-Efficient Cellular Communications With Coexistent One- and Two-Hop Transmissions," *IEEE Trans. Veh. Technol.*, vol. 65, no. 8, pp. 6765–6772, Aug. 2016.

[37] K. Song, B. Ji, Y. Huang, M. Xiao, and L. Yang, "Performance Analysis of Heterogeneous Networks With Interference Cancellation," *IEEE Trans. Veh. Technol.*, vol. 66, no. 8, pp. 6969–6981, Aug. 2017.

[38] K. Song, B. Ji, C. Li, and L. Yang, "Outage analysis for simultaneous wireless information and power transfer in dual-hop relaying networks," *Wirel. Networks*, vol. 25, no. 2, pp. 837–844, Feb. 2019.

[39] G. L. Stuber, "Principles of Mobile Communication". *Cham: Springer International Publishing*, 2017.

[40] C. Di Franco and G. Buttazzo, "Energy-Aware Coverage Path Planning of UAVs," in *2015 IEEE International Conference on Autonomous Robot Systems and Competitions*, 2015, pp. 111–117.

[41] Y. Chen, K. T. Sabnis, and R. A. Abd-Alhameed, "New Formula for Conversion Efficiency of RF EH and Its Wireless Applications," *IEEE Trans. Veh. Technol.*, vol. 65, no. 11, pp. 9410–9414, Nov. 2016.

[42] Y. Chen, N. Zhao, and M.-S. Alouini, "Wireless Energy Harvesting Using Signals From Multiple Fading Channels," *IEEE Trans. Commun.*, vol. 65, no. 11, pp. 5027–5039, Nov. 2017.

[43] I. S. Gradshteyn, *Tables of Integrals, Series, and Products*, Seventh Edition, vol. 56, no. 10. New York, USA: American Journal of Physics, 2007.

[44] O. Arnold, F. Richter, G. Fettweis, and O. Blume, "Power Consumption Modeling of Different Base Station Types in Heterogeneous Cellular Networks," in Future Network and Mobile Summit, 2010, pp. 1–8.